Diyala Journal of Engineering Sciences

Journal homepage: https://djes.info/index.php/djes

ISSN: 1999-8716 (Print); 2616-6909 (Online)

Optimizing Plate Adhesion: A Model Using Digital Image Correlation and Finite Element Analysis

Zahraa M. Gafil, Zaid S. Hammoudi*

Department of Mechanical Engineering, University of Diyala,32001 Diyala, Iraq

ARTICLE INFO

Article history:
Received: 24/12/2024.
Revised: 27/03/2025.
Accepted: 13/04/2025.
Available online: 15/06/2026

Keywords:
Single-Lap Joints
Adhesive Bonding
Finite Element Analysis (FEA)
Digital Image Correlation (DIC)

ABSTRACT

The durability and strength of single-lap adhesive joints are influenced by numerous factors. Among which are stress and strain concentrations at the overlap edges. This research investigates a method for improving these joints through a proposed geometric design incorporating a circular overlap region with a central hole. The primary objective is to reduce strain concentrations within the adhesive layer, which is an important factor governing joint strength and durability. An aluminum alloy was employed as the adherent material, in conjunction with an epoxy adhesive. Numerical and experimental analyses, utilizing the Finite Element Method (FEM) and Digital Image Correlation (DIC) techniques, were used to evaluate strain distribution and validate the proposed design. Three models of different inner circle diameter were tested. The tested where made such that the adherent area are the same of corresponding conventional rectangular area. Results indicate that the modified configuration achieved a reduction in normal strain within the adhesive layer ranging from 2.8% to 8.6% compared to the conventional design. Furthermore, strain concentrations at the overlap edges were redistributed, promoting a more uniform stress distribution and potentially enhancing joint strength. Very good agreement was observed between FEM and DIC results, varying from 69% to 95%, with an average exceeding 80% for most measurement points. These findings demonstrate the possibility of simple geometric modifications to enhance adhesive joint performance.

1. INTRODUCTION

The development of efficient and flexible joining methods for structures is crucial in cost-effective manufacturing as well as in the repair and replacement of components across various industries. Common joining technologies include mechanical fastening, welding and adhesive bonding, which offers significant advantages for joining metals compared with resistance spot welding or mechanical fasteners, such as rivets or screws. These advantages include its suitability for bonding dissimilar metals, low-temperature processing, combination of bonding and sealing in one operation, thermal and electrical insulation, uniform stress distribution, smooth surface appearance and improved fatigue, vibration and sound damping. Moreover, it reduces weight in many applications and simplifies structural design [1,2].

Among the adhesive options, epoxies stand out due to their versatility and adaptability. Epoxies provide good to excellent bonding with metals such as steel, aluminium and copper, offering a wide range of applications [1]. The adhesive used in this study is 4 Mins steel epoxy, a fast-curing, steel-filled epoxy adhesive. It features high bond strength and thermal resistance up to 120 °C, with an initial curing time of approximately four to five minutes. This epoxy exhibits a shear strength of no less than 90 kg/cm², as specified by the manufacturer [3].

Single-lap adhesive joint (SLJ), the most commonly used configuration owing to their simple geometry and high structural efficiency, face significant challenges. The primary drawback is load eccentricity, which induces bending in the adherends and results in high peel stress/strain at the adhesive edges. These stress concentrations arise from the substantial stiffness difference between the adhesive and adherends, reduced adhesive thickness and the applied load's nature [4,5].

To address these issues, research efforts have been directed into two strategies, material modifications and geometrical modifications. Material modifications involve enhancing adhesive ductility, for instance through rubber toughening. Whereas geometrical

* Corresponding author's E-mail: zshaaa@yahoo.com
DOI: 10.24237/djes.2026.19209

modifications focus on altering the shape of the adherend and/or adhesive, such as through the introduction of tapers, notches, or optimised profiles. For example, while increasing adhesive thickness can reduce peak stresses, it may compromise overall joint strength. Extending the overlap length improves load distribution but at the expense of increased shear stresses [6]. Chamfering adherends at specific angles (e.g., 15°) has been demonstrated to reduce peel stress and enhance load transfer efficiency [7]. Similarly, the incorporation of fillets at joint edges improves peel and shear strength by permitting a more uniform stress distribution [8,9]. Geometrical configurations, including recessed or hollow adherends, have demonstrated superior stress distribution and improved joint strength. Rounded or recessed geometries are effective in minimising peel stresses, whereas tapered geometries showed reducing of shear stresses [10]. Hybrid joints, which combine adhesive bonding with mechanical fastening, resulted superior performance [11]. The use of hollow adherends in bonding regions reduces stress peaks and enhances joint durability [12]. Finite Element Modelling (FEM) has been used in optimising Single-Lap Joint (SLJ) designs. FEM studies have shown, for instance, that the addition of spew fillets decreases stress concentrations and increases load-carrying capacity [13]. Numerical analysis of parameters such as adhesive and substrate thickness markedly affect stress and strain concentrations, with thinner adhesives generally showed more uniform distributions [14]. Experimental validation using Digital Image Correlation (DIC) has confirmed these numerical findings [15].

The present study focuses on strain at the overlap edge and within the adhesive layer, regions identified as critical for failure initiation [6-8]. AA2024-T3 aluminium alloy was selected for the adherends due to its low density and high corrosion resistance [16].

A comparative analysis was performed between a conventional SLJ configuration and a modified design featuring a circular overlap region with a central hole. The effect of this modified design on strain distribution within the adhesive and at the overlap edge was investigated. A steel mould was constructed and employed to ensure uniform adhesive thickness. Strain measurements were obtained using DIC, with subsequent image analysis performed using Ncorr, an open-source DIC software package, to evaluate strain distribution across both traditional and modified SLJ samples. FEM models ware developed in ANSYS Workbench 18.2 to study stress and strain distributions. Experimental tensile tests were performed at a loading speed of 1 mm/min using a testing machine equipped with a 50 kN load cell. Strain concentrations were quantified following deformation using DIC. The experimental results were then compared with FEM simulations to provide detailed insights into the influence of the modified geometry on strain concentrations relative to the conventional SLJ design.

2. METHODOLOGY

The objective of this study is to analyze strain concentrations at the overlap edges and within the adhesive layer. Where these regions identified as critical for failure initiation [6-8]. The experimental methodology employs Digital Image Correlation (DIC) to measure full-field strain distributions under tensile loading. Finite Element Method (FEM) simulations are conducted to compute strains and validate experimental findings. The influence of geometric modifications on strain concentrations and overall joint strength is analyzed.

2.1 Sample Preparation

AA2024-T3 aluminium alloy was selected as the adherent material. It is commonly used in industrial applications. Also, aluminum has relatively low modulus of elasticity, thus higher deformation and strain compared to other materials like steel. The high strain values facilitate strain measurement by DIC. An epoxy adhesive was chosen for its high bonding strength and proven compatibility with aluminium substrates.

Aluminium plates were machined to the required geometry using a computer numerical control (CNC) cutting machine. spacemen dimensions are width w = 30 mm, adherent thickness t = 1 mm, and adherent length l = 100 mm. The adhesive layer thickness was maintained at t_s = 0.5 mm, as illustrated in Figure 1. This specific adhesive thickness was selected based on prior studies which indicate that a range of 0.1–0.5 mm is optimal for achieving maximum joint strength [14]. A thickness of 0.5 mm was therefore employed to align with these recommendations and ensure optimal adhesive performance [6,14]. The selection of the higher limit of adhesive thickness enables better analysis of strain at edges by DIC.

To ensure a contaminant-free surface prior to bonding, each sample was cleaned with acetone to remove oils and contaminants, followed by a water rinse and drying. A calibrated steel spacer and a custom-designed mould were utilised to guarantee a consistent bond line thickness. The mould assembly is shown in Figure 2. It consisted of upper and lower steel plates clamped together using bolts and nuts. Two metallic spacers, each with a thickness of 2.5 mm, were positioned on either side of the aluminium plates. The 1 mm-thick aluminium adherends were positioned centrally within the mould with the adhesive applied between them. Upon clamping, the combined thickness of the adherends (2 mm) and the adhesive layer (0.5 mm) equalled the total spacer thickness. Thereby ensuring precise control over the adhesive layer thickness throughout the curing process.

The modified SLJ design is simply making the overlap area's edge as a half circle, and placing hole in the overlap area. The aim is to reduce the strain concentration. Three hole diameters were used: *di=17, 18* and *19 mm*, with two samples prepared for each diameter.

The selection of these hole diameters was based on a parametric study conducted using the FEM. Various hole diameters were analysed to assess their effect on strain distribution at the overlap edge and within the adhesive layer. The results demonstrated that these specific diameters resulted in the lowest longitudinal strain in the adhesive layer, minimising strain concentrations and enhancing the joint's mechanical performance. The parametric study further confirmed that reducing the hole diameter below 17 mm increased strain concentrations at the overlap edge, whereas the selected diameters exhibited a more favourable strain distribution with reduced longitudinal strain in the adhesive layer.

The adhesive bond area in each case is computed. The conventional SLJ area is adjusted, and the corresponding suggested areas are equated. The overlap lengths are *lo*= 16, 15.08 and 14.11 mm.

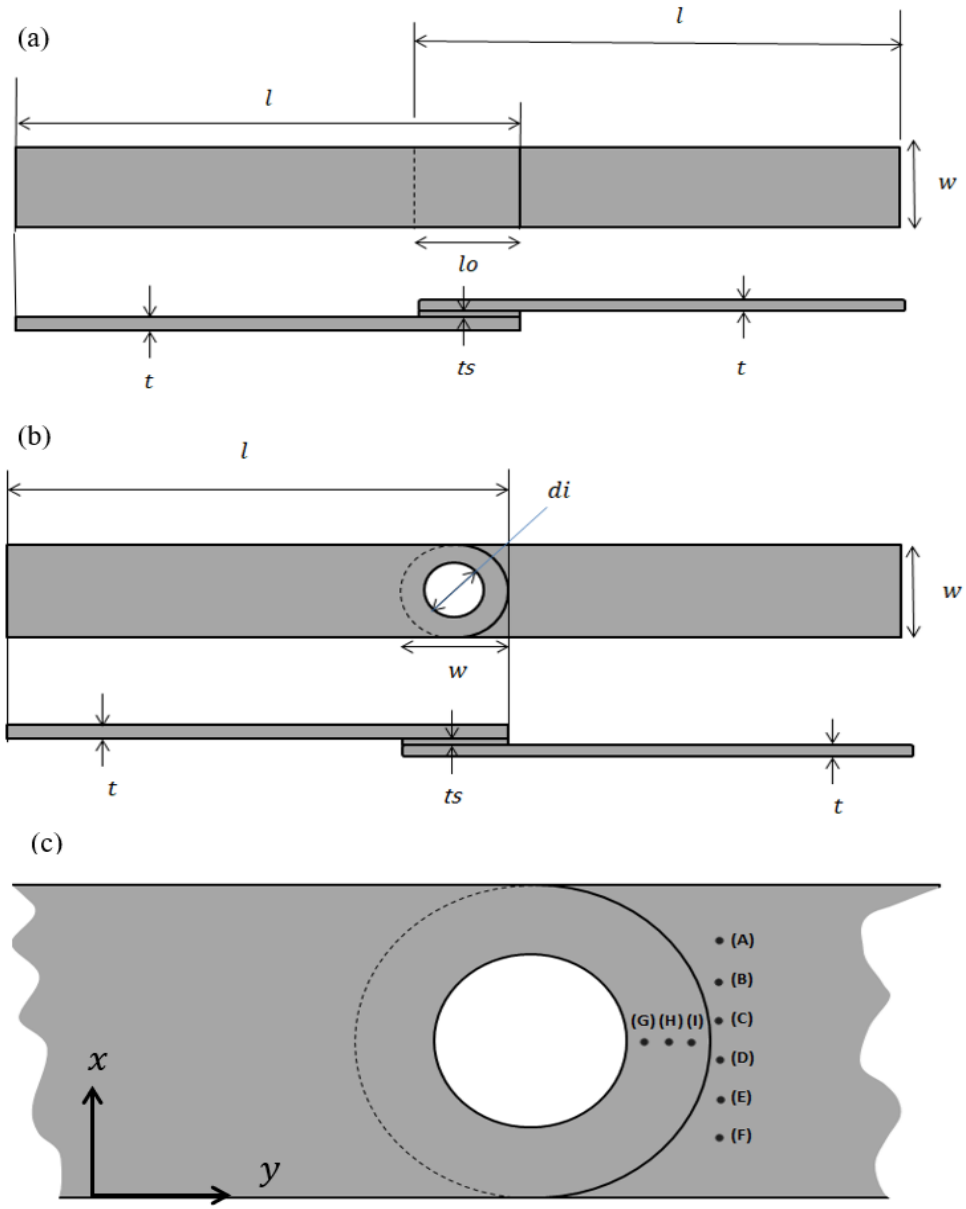

Figure 1. Schematic representation of single-lap joint designs: (a) conventional SLJ (b) modified SLJ (c) position of points analyzed

2.2 Experimental Setup (DIC)

Digital Image Correlation (DIC) is a non-contact optical technique employed to measure strain and deformation distribution on a material surface through the analysis of digital images. The procedure is initiated by capturing a reference image of the unloaded specimen, followed by a sequence of images acquired during deformation. As the material deforms, the applied speckle pattern on its surface undergoes displacement relative to the reference image. Correlation algorithms

analyze pixel intensity variations to compute full-field displacement and strain measurements [17]. A principal advantage of DIC is its capacity to provide precise, high-resolution strain measurements across the entire sample surface. It is capable of providing better accuracy than other experimental methods—such as ultrasonic testing, acoustic emission, and thermography—DIC regarding strain measurements in critical regions of the sample [18-20]. Accurate application of DIC requires the preparation of the specimen surface with a high-quality random speckle pattern. To achieve this, the surface was first cleaned, then coated with a white base layer to ensure high contrast. Lastly, black dots were applied randomly using a fine spray can. This process ensured that the speckle pattern remained adherent to the surface and deformed congruently with the specimen during loading. The prepared specimen was then securely mounted in a tensile testing machine, with careful attention to alignment to minimize out-of-plane displacements that could compromise measurement accuracy. Image acquisition was performed using a 20-megapixel industrial camera equipped with a 75 mm lens, selected for its high resolution and rapid data transfer capabilities. Uniform illumination was maintained across the specimen surface using white LED lights covered by diffusers.

The camera was positioned parallel to the specimen surface at a fixed distance for the duration of the experiment. An initial reference image was captured prior to loading, with subsequent images acquired under applied tensile force. These images were analyzed to calculate strain distributions, with particular emphasis on normal strain like longitudinal strain (ε_yy). Additionally, von Mises strain was analyzed to provide a comprehensive understanding of the overall strain distribution across the adhesive joint. In a 2D DIC system, the coordinates of a tracked point prior to loading are defined as (x_p, y_p), with the new position following deformation denoted as (x_p′, y_p′). The image is partitioned into a grid of subsets, and displacements and strains are computed with good precision by tracking positional changes before and after loading. Figure 3 illustrates the working principle of DIC. It shows working reference subset prior to deformation and the target subset after loading. Leading to a clear visualization of the displacement [21]. Image analysis and strain measurement were performed using the open-source Ncorr software, which is developed on the MATLAB platform. This software offers a cost-effective alternative to commercial post-processing tools. It is applicable to various materials that can maintain a fine speckle pattern under loading conditions. Two samples were prepared for each test case, and the average strain values were considered to ensure reliable results. Figure 5 illustrates the experimental setup, and Figure 4 presents the applied speckle pattern on the SLJ specimens.

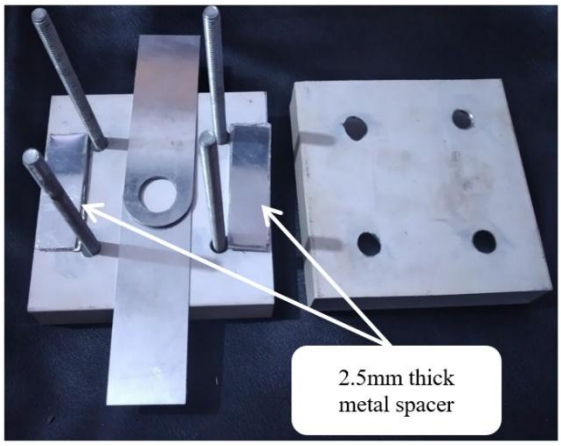

Figure 2. Steel Mold for Adhesive Thickness Control

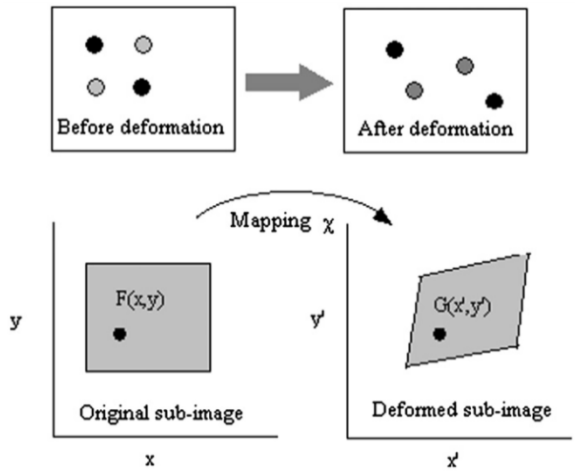

Figure 3. Digital image correlation deformation working principle [21].

Figure 4. Speckle Pattern Applied on SLJ Specimens

2.3 Finite Element Analysis (FEA)

FEM was developed using ANSYS Workbench 18.2 to simulate strain distribution under a uniaxial tensile load of 800 N. The analysis focused on capturing the strain concentrations at the adhesive layer whilst ensuring computational efficiency and numerical accuracy.

A mesh convergence analysis was conducted for the SLJ to determine the optimal element size that ensures strain values are independent of mesh density. A series of simulations was performed using different mesh sizes, evaluating their effects on the extracted strain values. The results indicated that reducing the element size to 0.08 mm led to noticeable changes in the strain values, beyond which further refinement had a negligible impact. Consequently, this element size was selected as the optimal mesh size, providing a balance between computational accuracy and numerical efficiency. This analysis confirms that the selected mesh achieves reliable numerical convergence, ensuring that the strain values are not influenced by mesh variations, as shown in Figure 7.

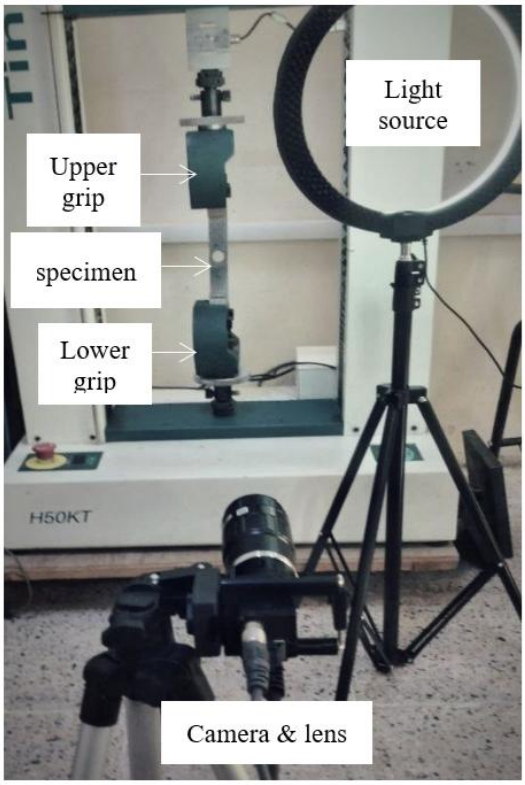

Figure 5. Experimental setup for strain measurement involving 2D DIC

The boundary conditions in the FEM were applied to replicate those used in the physical test. The lower end of the specimen was fully fixed to prevent any movement in all directions, whereas the upper end was constrained from movement in the X and Z directions using displacement boundary conditions, as shown in Figure 6. This setup ensures an accurate representation of the specimen's behaviour under tensile loading. A uniaxial tensile force of 800 N was applied uniformly across the top surface of the specimen, simulating the experimental conditions [22,23].

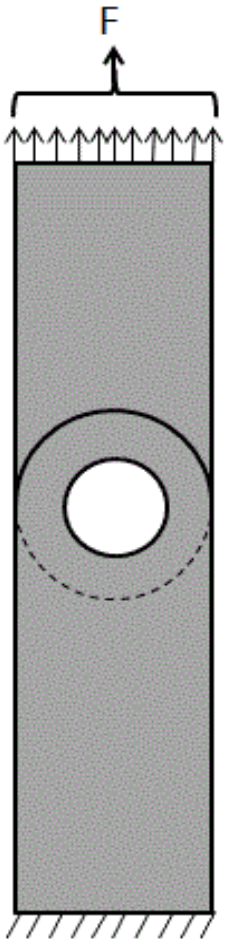

Figure 6. Boundary Conditions of SLJ

The meshing strategy involves the use of hexahedral elements in the region outside the overlap zone due to its well-defined geometric shape. By contrast, tetrahedral elements were used in the overlap region and adhesive layer due to the presence of a central hole, which required a more flexible meshing approach. This hybrid meshing strategy effectively captured localised strain gradients whilst maintaining computational efficiency.

The mechanical behaviour of both materials was assumed to be linear elastic, as the applied load remained within the elastic deformation region for the aluminium and epoxy adhesive. The mechanical properties of the aluminium adherends were experimentally determined through uniaxial tensile testing, ensuring accurate representation in the model. Meanwhile, the mechanical properties of the epoxy adhesive, such as Young's modulus and Poisson's ratio, were obtained from the official specifications provided by the adhesive manufacturer. These properties, summarised in Table 1, were used as input parameters for the finite element analysis.

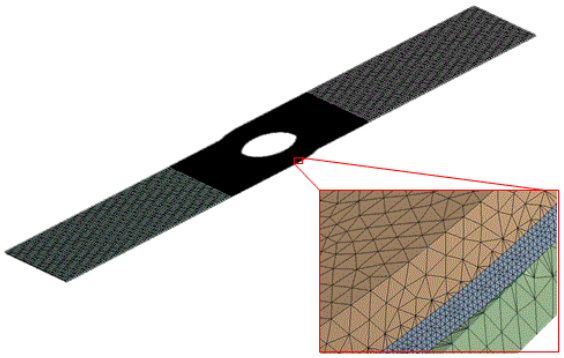

Figure 7. Finite element mesh adopted in the present study

Table 1. Mechanical properties of material in FEM anslysis

Material	Young's Modulus (MPa)	Poisson's Ratio
Aluminium	69,000	0.33
Epoxy Adhesive	2,500	0.33

3. RESULTS AND DISCUSSION

3.1 Analysis of Conventional SLJ

3.1.1 FEA

FEA was used to examine strain distribution in conventional (SLJ) designs with overlap lengths of 16, 15.08 and 14.11 mm. The analysis focused on maximum longitudinal strain (*Eyy*) in the adhesive layer and at the overlap edge, which are critical regions of deformation. The von Mises strain was also evaluated as an indicator of the overall strain distribution.

FEM Results and Analysis:

- 16 mm overlap length:
  - Maximum *Eyy*in adhesive layer: 2.72e-3.
  - Maximum *Eyy*at overlap edge: 2.37e-3 (Figure 8a).
  - Von Mises strain: 2.27e-2.

These results indicate that the adhesive layer experiences the highest strain near the overlap edge due to the concentration of forces at the boundary. Thus, this region becomes critical for potential failure under tensile loading. The observed strain distribution suggests that longer overlap lengths enhance load sharing across the joint, reducing localised strain concentrations and improving joint performance.

- 15.08 mm overlap length:
  - Maximum *Eyy* in adhesive layer: 2.69e-3.
  - Maximum *Eyy* at overlap edge: 2.38e-3 (Figure 9a).
  - Von Mises strain: 2.21e-2.

Interpretation: A slight reduction in overlap length increases strain concentration at the overlap edges due to the reduced contact area. Nevertheless, the overall strain intensity within the adhesive layer remains comparable because the majority of the load continues to be distributed across the adhesive region.

This finding further highlights the critical importance of edge behaviour in determining joint performance.

- 14.11 mm overlap length:
  - Maximum *Eyy* in adhesive layer: 2.69e-3.
  - Maximum *Eyy* at overlap edge: 2.38e-3 (Figure 10a).
  - Von Mises strain: 2.13e-2.

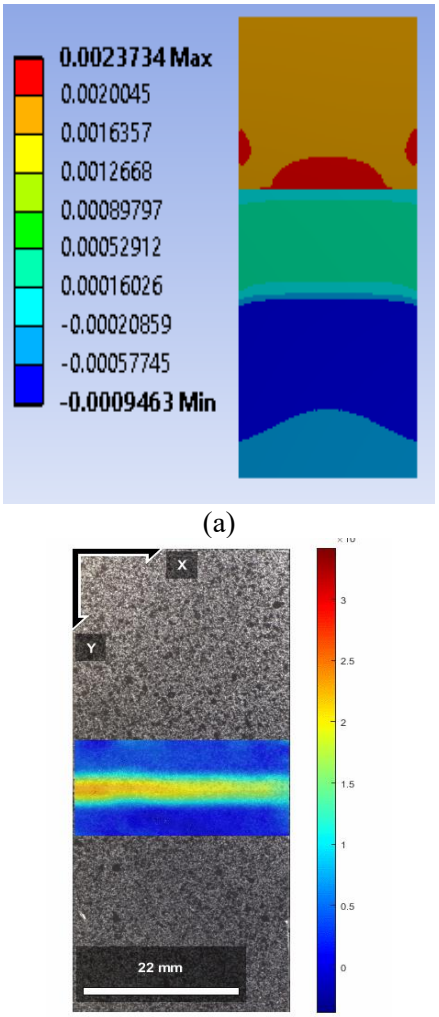

Figure 8. Longitudinal strain eyy at overlap length 16mm (a) FEM (b) DIC

The shortest overlap length exhibits the highest strain concentrations at the overlap edge, considerably reducing the durability and strength of the joint under repeated loading. This behaviour is attributed to the minimised load transfer area, leading to a higher stress intensity at critical points compared with longer overlap lengths.

The analysis consistently demonstrated strain concentration near the overlap edge across all configurations. Whilst shorter overlap lengths slightly increased *Eyy* near the edge, they also redistributed strain intensity within the adhesive layer, indicating a trade-off between edge behavior and overall strain distribution. These findings can guide the design of optimised joint geometries that balance load distribution with edge strain minimisation.

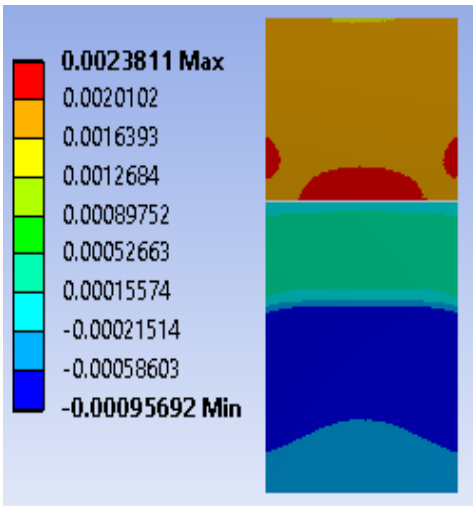

(a)

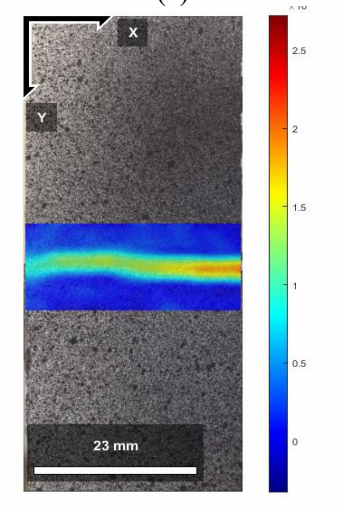

(b)

Figure 9. Longitudinal strain ε_{yy} at overlap length 15.08mm (a) FEM (b) DIC

3.1.2 DIC Analysis

DIC was used to measure longitudinal strain (Eyy) at the overlap edge for the same overlap lengths.

- 16 mm overlap length:
  - The longitudinal strain Eyyat the overlap edge is 2.49e-3 (Figure 8b).

This value closely matches the FEM predictions, highlighting the strain concentration near the overlap edge. The relatively longer overlap length provides improved load distribution across the adhesive layer, reducing the strain concentration at the edge and enhancing the joint's overall performance.

- 15.08 mm overlap length:
  - The longitudinal strain Eyyat the overlap edge is 2.58e-3 (Figure 9b).

The result shows slight increase in strain compared with the 16 mm overlap length using FEM, emphasising the impact of reduced overlap length on strain concentration at the edge. This result underscores the sensitivity of joint performance to the overlap length, where shorter lengths lead to higher strain concentrations.

- 14.11 mm overlap length:
  - The longitudinal strain Eyyat the overlap edge is 2.61e-3 (Figure 10b).

This increase in strain value compared with longer overlap lengths indicates a more pronounced strain concentration at the edge due to the limited load-bearing area. The findings align well with FEM results, reaffirming the critical role of edge strain behaviour in influencing the structural performance of adhesive joints.

These results confirm the effectiveness of DIC in capturing localised strain variations, providing experimental validation for FEM simulations. The progressive increase in edge strain with decreasing overlap length highlights the importance of optimising overlap geometry to balance strain distribution and improve joint reliability.

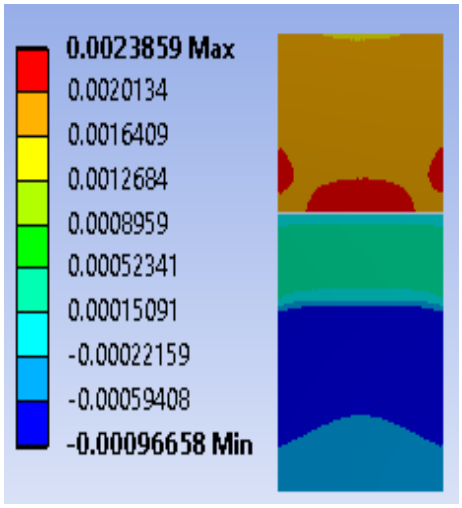

(a)

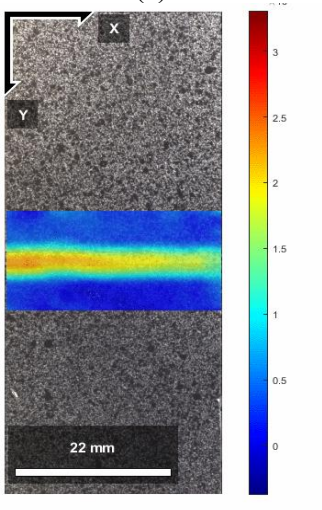

(b)

Figure 10. Longitudinal strain ε_{yy} at overlap length 14.11mm (a) FEM (b) DIC

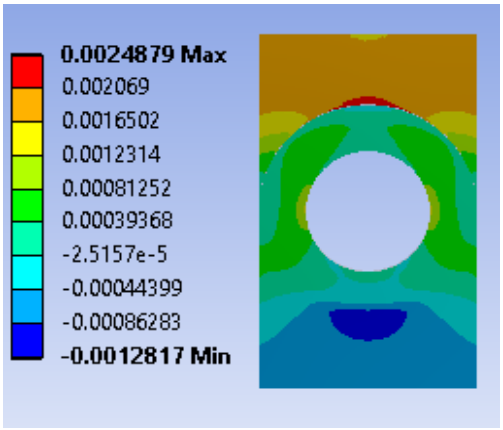

(a)

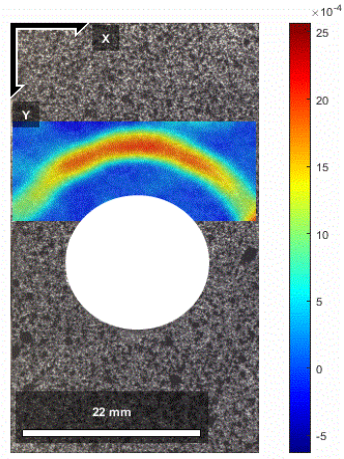

(b)

Figure 11. Longitudinal strain ε_{yy} at 17mm hole diameter (a) FEM (b) DIC

3.2 Analysis of Modified SLJ Design

3.2.1 FEM Analysis

Modified (SLJ) designs with circular overlap regions and central holes of diameters 17, 18 and 19 mm were analysed. The bonding areas were adjusted to match those of conventional SLJ to ensure consistent comparison. The percentage improvements between the conventional and modified joints are shown in Table 2.

- 17 mm Diameter:
  - Maximum longitudinal strain *Eyy* in the adhesive layer is 2.64e-3 (+2.88% compared with the 16 mm overlap).
  - Maximum longitudinal strain *Eyy* at the overlap edge is 2.48e-3 (−4.81% compared with the 16 mm overlap), as shown in Figure 11a.
  - Von Mises strain is 2.29e-2 (−0.61%).
  - Interpretation: Introducing a central hole reduces the overall strain in the adhesive layer whilst slightly minimising the strain at the overlap edge, indicating a balance in strain redistribution.
- 18 mm Diameter:
  - Maximum longitudinal strain *Eyy* in the adhesive layer is 2.50e-3 (+7.06% compared with the 15.08 mm overlap).
  - Maximum longitudinal strain *Eyy* at the overlap edge is 2.36e-3 (+0.72% compared with the 15.08 mm overlap), as shown in Figure 12a.
  - Von Mises strain is 2.37e-2 (−7.30%).
  - Interpretation: Increasing the hole diameter further reduces the strain in the adhesive layer, enhancing joint performance whilst slightly decreasing the von Mises strain.
- 19 mm Diameter:
  - Maximum longitudinal strain *Eyy* in the adhesive layer is 2.46e-3 (+8.57% compared with the 14.11 mm overlap).
  - Maximum longitudinal strain *Eyy* at the overlap edge is 2.36e-3 (+0.72% compared with the 14.11 mm overlap), as shown in Figure 13a.
  - Von Mises strain is 2.20e-2 (−3.22%).
  - Interpretation: The largest hole diameter achieves the greatest reduction in adhesive layer strain, with minimal impact on the overlap edge strain, demonstrating its effectiveness in improving joint performance.

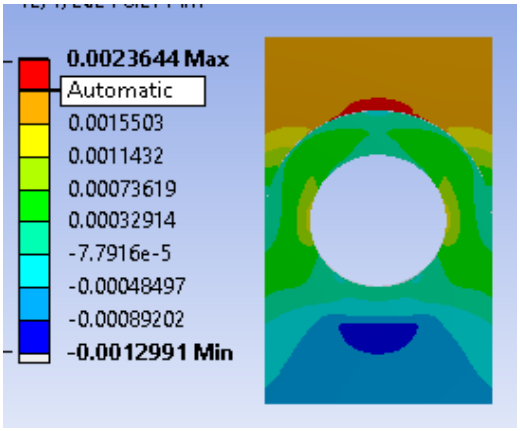

(a)

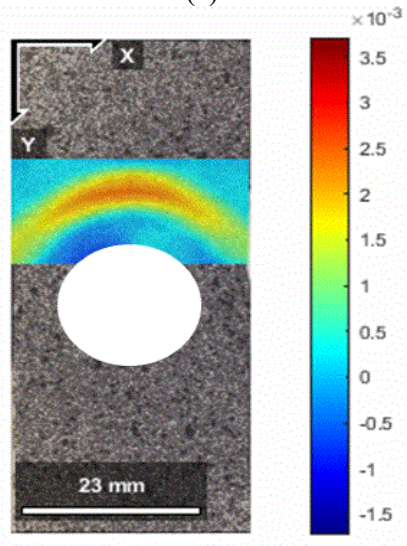

(b)

Figure 12. Longitudinal strain ε_{yy} at 18mm hole diameter (a) FEM (b) DIC

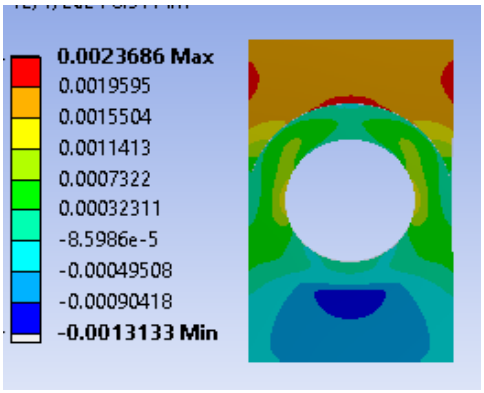

(a)

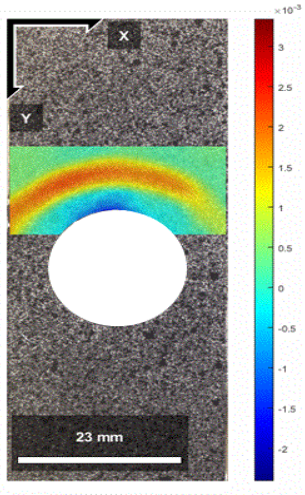

(b)

Figure 13. Longitudinal strain ε_{yy} at 19mm hole diameter (a) FEM (b) DIC

3.2.2 DIC Analysis

DIC measurements for modified SLJ designs provided additional validation for FEM findings.

Summary of DIC Results:

- 17 mm Diameter: ε_{yy} = 2.46e-3 (Figure 11b).
  - Interpretation: DIC analysis confirms the FEM-predicted reduction in adhesive layer strain, validating the modification.
- 18 mm Diameter: ε_{yy} = 2.34e-3 (Figure 12b).
  - Interpretation: Consistent with FEM results, the reduction in strain demonstrates the benefits of increasing the hole diameter.
- 19 mm Diameter: ε_{yy} = 2.32e-3 (Figure 13b).
  - Interpretation: The DIC findings support FEM predictions, showing that the largest hole diameter yields the most significant strain reduction in the adhesive layer.

DIC results closely matched FEM predictions, highlighting the effectiveness of the modified design in reducing strain concentrations.

3.3 Agreement between FEM and DIC Analysis

In this section, the longitudinal strain (ε_{yy}) results obtained using FEM and DIC are compared at nine specific points with distinct coordinates, as illustrated in Figure 1c. These points are labelled as A, B, C, D, E, F, G, H and I. The coordinates are defined relative to the origin point (0, 0, 0), located at the centre of Figure 1b.

For the DIC results, two samples were analysed for each point size, and the average strain values were calculated. The agreement ratio percentage between FEM and DIC results was determined using the following equation:

$$Agreementratio = \left(1 - \left|\frac{FEM-DIC}{FEM}\right|\right) * 100\%.$$

The FEM and Avg DIC results, as well as the calculated agreement ratios for all nine points, are summarised in Table 3.

The results indicate a high level of agreement between FEM and DIC, with agreement ratios exceeding 80% for most points, demonstrating the reliability of the FEM predictions when compared with experimental measurements. However, the last point (Point I) shows the lowest agreement ratio, which could be attributed to experimental inaccuracies or model limitations.

The low agreement at points I between the FEM and DIC results can be attributed to inherent imperfections in the experimental process and potential sources of error in measurement and analysis. Several factors may contribute to this discrepancy, including issues with the speckle pattern, where uneven distribution or low contrast could affect displacement and strain accuracy. Calibration inaccuracies in the camera or DIC system may also introduce variations in displacement calculations, particularly in regions with complex deformation. In addition, material interaction effects at point I, influenced by nonlinear adhesive–adherent interactions, add complexity to its behaviour, causing difficulty to capture accurately in numerical models. Surface irregularities, such as small defects or inconsistencies in specimen coating, may alter the local strain response, leading to deviations in DIC measurements. Furthermore, optical conditions, including lighting variations and surface reflections, can impact measurement accuracy, causing localised discrepancies between DIC and FEM results. Given these factors, the low agreement at point I can be explained by the inherent limitations of experimental techniques, which are susceptible to various sources of error and inconsistencies, resulting in localised deviations from numerical simulation results.

Table 2. improvements result when using modified design

Modified Joint hole diameter (mm)	Longitudinal Strain Improvement ε_{yy} in Adhesive Layer (%)	Longitudinal Strain Improvement ε_{yy} at Overlap Edges (%)	Von Mises Strain Improvement (%)
17	+2.88%	-4.84%	-0.61%
18	+7.06%	+0.72%	-7.30%
19	+8.57%	+0.73%	-3.22%

Table 3. Comparison of FEM and Average DIC Longitudinal Strain ε_{yy} Results at the Overlap Edge.

Point	Coordinates (x,y,z) mm	FEM ε_{yy}	DIC ε_{yy}	Agreement Ratio (%)
A	(10, 16, 0.25)	1.782e-3	1.44e-3	80.81
B	(6, 16, 0.25)	1.8699e-3	2.28e-3	78.07
C	(2, 16, 0.25)	2.0453e-3	2.33e-3	86.08
D	(-2, 16, 0.25)	2.0452e-3	2.4e-3	82.65
E	(-6, 16, 0.25)	1.8703e-3	2.31e-3	76.49
F	(-10, 16, 0.25)	1.7814e-3	1.98e-3	88.85
G	(0, 12, -1.25)	3.406e-4	3.109e-4	91.28
H	(0, 13, -1.25)	2.5569e-4	2.68e-4	95.19
I	(0, 14, -1.25)	2.9759e-6	2.05e-3	68.8

4. CONCLUSIONS

4.1 Analysis of Conventional SLJ

- FEA results indicated that the adhesive layer experiences maximum strain at the overlap edge.
- Reducing the overlap length increased strain concentration at the edges, potentially affecting load-bearing capacity and durability.
- DIC confirmed the longitudinal strain measurements at the overlap edge, exhibiting strong agreement with FEA results.

4.2 Analysis of the Modified SLJ Design

- Modified SLJ designs, incorporating a circular overlap region with a central hole of 17, 18 and 19 mm, were analysed.
- The results demonstrated an improvement in strain distribution and a reduction in maximum longitudinal strain in the adhesive layer, with a peak reduction of 8.57% compared with the conventional SLJ.
- The high-strain region was significantly reduced in the modified design, leading to improved stress distribution.

4.3 Comparison between FEA and DIC Results

Strain measurements were analysed at nine specific points using FEA and DIC.

- The results suggested a high correlation between the two methods, with agreement ratios exceeding 80% in most cases, confirming the accuracy of the numerical model.
- The lowest agreement ratio was observed at one measurement point, which may be attributed to experimental inaccuracies or limitations in the numerical model.

REFERENCES

[1] S. Maggiore, et al., "A review of structural adhesive joints in hybrid joining processes," Polymers, vol. 13, no. 22, p. 3961, 2021. https://doi.org/10.3390/polym13223961

[2] M. D. Banea, "Influence of adherend properties on the strength of adhesively bonded joints," MRS Bulletin, vol. 44, pp. 625–629, 2019. https://doi.org/10.1557/mrs.2019.180

[3] 4 MINS STEEL EPOXY: www.xtraseal.com

[4] E. M. Moya-Sanz, I. Ivañez, and S. K. Garcia-Castillo, "Effect of the geometry in the strength of single-lap adhesive joints of composite laminates under uniaxial tensile load," International Journal of Adhesion and Adhesives, vol. 72, pp. 23–29, 2017. https://doi.org/10.1016/j.ijadhadh.2016.10.009

[5] S. L. S. Nunes, R. D. S. G. Campilho, F. J. G. da Silva, C. C. R. G. de Sousa, T. A. B. Fernandes, M. D. Banea, and L. F. M. da Silva, "Comparative failure assessment of single and double-lap joints with varying adhesive systems," The Journal of Adhesion. https://doi.org/10.1080/00218464.2015.1103227

[6] L. M. Fernández-Cañadas, et al., "Effect of adhesive thickness and overlap on the behavior of composite single-lap joints," Mechanics of Advanced Materials and Structures, vol. 28, no. 11, pp. 1111–1120, 2021. https://doi.org/10.1080/15376494.2019.1639086

[7] E. M. Moya-Sanz, I. Ivañez, and S. K. Garcia-Castillo, "Effect of the geometry in the strength of single-lap adhesive joints of composite laminates under uniaxial tensile load," International Journal of Adhesion and Adhesives, vol. 72, pp. 23–29, 2017. https://doi.org/10.1016/j.ijadhadh.2016.10.009

[8] G. Zheng, et al., "Effect of spew fillet on adhesively bonded single lap joints with CFRP and aluminum-alloy immersed in distilled water," International Journal of Adhesion and Adhesives, vol. 99, article 102590, 2020. https://doi.org/10.1016/j.ijadhadh.2020.102590

[9] M. O. Doru, et al., "Effect of the spew fillet on adhesively bonded single-lap joint subjected to tensile loading: experimental and 3-D non-linear stress analysis," The Journal of Adhesion, vol. 90, no. 3, pp. 195–209, 2014. https://doi.org/10.1080/00218464.2013.777900.

[10] Calik, "Effect of adherend shape on stress concentration reduction of adhesively single lap joint," Engineering Review, vol. 34, no. 4, pp. 315–322, 2017.

[11] M. Shishesaz and M. Hosseini, "Effects of joint geometry and material on stress distribution, strength and failure of bonded composite joints: an overview," The Journal of Adhesion, 2020. https://doi.org/10.1080/00218464.2018.1554483

[12] F. Marchione, "Effect of hollow adherends on stress peak reduction in single-lap adhesive joints: FE and analytical analysis," The Journal of Adhesion, vol. 98, no. 6, pp. 656–676, 2022. https://doi.org/10.1080/00218464.2021.1995368

[13] M. O. Doru, et al., "Effect of the spew fillet on adhesively bonded single-lap joint subjected to tensile loading: experimental and 3-D non-linear stress analysis," The Journal of Adhesion, vol. 90, no. 3, pp. 195–209, 2014.

[14] Akhavan-Safar, M. R. Ayatollahi, and L. F. M. da Silva, "Strength prediction of adhesively bonded single lap joints with different bondline thicknesses: A critical longitudinal strain approach," International Journal of Solids and Structures, vol. 109, pp. 189–198, 2017. https://doi.org/10.1016/j.ijsolstr.2017.01.022

[15] F. Ramezani, et al., "A comprehensive experimental study on bi-adhesive single lap joints using DIC technique," International Journal of Adhesion and Adhesives, vol. 102, article 102674, 2020. https://doi.org/10.1016/j.ijadhadh.2020.102674

[16] P. Samal, et al., "Recent progress in aluminum metal matrix composites: A review on processing, mechanical and wear

properties," Journal of Manufacturing Processes, vol. 59, pp. 131–152, 2020. https://doi.org/10.1016/j.jmapro.2020.09.010

[17] Pan, Bing, Kemao Qian, Huimin Xie, and Anand Asundi. "Two-dimensional digital image correlation for in-plane displacement and strain measurement: a review." Measurement science and technology 20, no. 6 (2009): 062001. DOI 10.1088/0957-0233/20/6/062001

[18] Berfield, T. A., J. K. Patel, R. G. Shimmin, P. V. Braun, J. Lambros, and N. R. Sottos. "Micro-and nanoscale deformation measurement of surface and internal planes via digital image correlation." Experimental Mechanics 47, no. 1 (2007): 51-62.

[19] McCormick, Nick, and Jerry Lord. "Digital image correlation." Materials today13, no. 12 (2010): 52-54. https://doi.org/10.1016/S1369-7021(10)70235-2

[20] Mukhtar, M. A. . Khattak, I. S. . Shahid, and M. S. M. . Sufian, "A Review on Application of Non Destructive Techniques on Composites", J. Adv. Res. Appl. Mech. , vol. 20, no. 1, pp. 12–21, Oct. 2020.

[21] Blaber, J., B. Adair, and A. Antoniou. "Ncorr: open-source 2D digital image correlation matlab software." Experimental Mechanics 55, no. 6 (2015): 1105-1122

[22] ASKER, HAVAL. "Numerical Optimization of the effect of the aspect ratio on the dynamic performance of plates." Journal of Duhok University 26.2 (2023): 671-681.

[23] Nobre, Jaoa Paulo, et al. "Stress Evaluation Through the Layers of a Fibre-Metal Hybrid Composite by IHD: An Experimental Study." Experimental Mechanics 64.4 (2024): 487-500.